

NEW CERAMIC MATERIALS FROM THE MELT FOR HIGH TEMPERATURE APPLICATIONS

N. Piquet, L. Mazerolles, M.F. Trichet

Centre d'Etudes de Chimie Métallurgique – CNRS, France

D. Boivin, M. Parlier

Office National d'Etudes et de Recherches Aérospatiales, France

1. Introduction

The improvement of energy efficiency and the reduction of polluting emission such as CO₂ and NO_x in some fields such as gas turbine and thermal power generation systems, require the use of new high-temperature structural materials exhibiting a tensile strength of at least a few hundreds MPa at temperatures above 1500°C, in air. For example, turbine blades and nozzles in the future engines would be made of lightweight, high-strength, high toughness and oxidation resistant materials at temperatures where metal superalloys, even coated by zirconia, would have already melted. The ceramic matrix composites consisting of silicon carbide fibers –or whiskers - embedded in a ceramic matrix, which were developed in the twenty last years, do not remain stable at temperatures higher than 1300°C in oxidizing atmosphere. Ceramic oxides could be potentially good candidates but up to now, brittleness of polycrystalline sintered materials, mainly due to the grain boundaries, limits their use. Melt growth composites (MGC) of oxides seem to be promising materials by coupling

two or three single crystal phases in a microstructure almost free of grain boundaries in addition to their intrinsic resistance to oxidation. About this class of material the challenge for future applications will be (i) to prepare, from binary or ternary systems, materials displaying minimal residual stresses arising from the different thermal expansion coefficients of constituent phases and (ii) to maintain a high flexural strength and a good fracture toughness at high temperatures. Waku et al [1, 2] have recently developed composites with microstructures consisting of interconnected networks of eutectic phases and exhibiting high flexural strength and good creep resistance. In this paper we will present results on similar microstructures obtained by directional solidification in different Al₂O₃ and Ln₂O₃ based systems. We investigated the effect of solidification conditions using two different crystal growth methods, the crystalline homogeneity of the as-prepared materials, and the role of the addition of a third phase (ternary systems) concerning the microstructure and the fracture toughness at room temperature.

2. Experimental procedures

2.1 Crystal growth

Under controlled conditions, solidification from the melt leads to materials free of porosity and with a very low amount of grain boundaries which are generally at the origin of brittleness in sintered ceramics. Furthermore directional solidification process often results in highly textured materials with well-defined crystallographic orientation relationships between the constituent phases [3]. Unidirectional solidification of based-oxide systems at eutectic composition usually leads to composites displaying an organized microstructure ranging from fibrous to lamellar depending upon the volume fractions of the eutectic phases [4,5]. The regular alignment of eutectic structures free of primary phase generally requires planar growth front conditions. Such conditions are met by using methods which allow high G/R values (G is the temperature gradient at the solid-liquid interface and R is the growth rate) [6]. These aligned fiber-type or lamellar microstructures give rise to a very strong anisotropic behaviour of these “*in situ*” composites which is not always wanted for good thermomechanical properties.

Other microstructures can be obtained in refractory oxide systems by unidirectional solidification such as continuous and isotropic networks of eutectic single-crystal phases which interpenetrate without grain boundaries. Synthesis of this class of materials as monoliths or fibers respectively in the Al₂O₃-Gd₂O₃ and Al₂O₃-Y₂O₃ systems was reported in recent papers [1,2,7]. The equipments that we used so far for the growth of oxide-oxide eutectics were made of high temperature single-crystal devices which display a high thermal gradient. Rods of oriented eutectics, of about 8mm in diameter, were grown using two different techniques:

(i) the floating-zone translation using an arc image furnace operating with a 6-kW xenon lamp as radiation source. Solidification

runs were achieved at various rates ranging between 2 and 20 mm.h⁻¹ [8].

(ii) the Bridgman method consisting in lowering, through a RF heated graphite susceptor, a molybdenum cylindrical crucible containing the powder mixture at the eutectic composition. The experiment was performed under a pressure of 10⁻⁵ mm.h⁻¹Hg of argon. The slowest solidification rate used with this technique was 14 mm.h⁻¹.

2.2 Microstructural and crystallographic characterization

Microstructural analysis was achieved on sections of rods parallel and perpendicular to the growth direction. These sections were cut using a diamond saw and their surfaces were polished to the micrometer scale using diamond paste. Samples, after Au-Pd coating, were examined by Scanning Electron Microscopy (SEM) using a Leo 1530 (Leo, Germany) equipped with a Princeton Gamma Tech (USA) EDX accessory. Backscattered electron contrast was used for these observations. Distribution of elements and compositions of eutectic phases were determined by EDX microanalysis. The structural analysis of the different phases and determination of the cell parameters were achieved from X-Ray powder patterns recorded with a PW 1830 Philips diffractometer (using the $\lambda=0.17889\text{nm}$ K_α radiation of cobalt). Growth directions and local relative orientations of phases were investigated from Transmission Electron Microscopy (TEM) observations performed on a Jeol 2000EX microscope (operating at 200kV). Thinned foils of transverse sections were prepared by mechanical dimpling and ion-milling. Electron backscattered diffraction (EBSD) was used to map the crystallographic orientations distribution and to determine the crystalline homogeneity of specimen. EBSD patterns were collected from a Zeiss DSM 960 microscope equipped with a tungsten filament and TSL analysis system. A step size of 0.5μm, was generally used. Measurements of the ratio of

the crack length to the Vickers indent size provided estimation of fracture toughness using the calibration curve developed by Marshall and Evans [9].

3. Results

3.1. Binary systems

The considered eutectic composites were prepared in the Al_2O_3 - Ln_2O_3 systems of which phase diagrams all display a eutectic composition at a temperature closed to 1800°C on the alumina rich side. Depending on the rare-earth oxide, eutectic phases consist in an Al_2O_3 phase which is associated to either LnAlO_3 ($\text{Ln}=\text{Sm}$, Eu , and Gd) or $\text{Ln}_3\text{Al}_5\text{O}_{12}$ for the other elements of the lanthanides serie. LnAlO_3 has a distorted perovskite structure (orthorhombic Pnma symmetry) and $\text{Ln}_3\text{Al}_5\text{O}_{12}$ crystallizes with a garnet-type structure (cubic Ia3d symmetry). Table I reports the unit-cell parameters of eutectic phases of various grown composites. SEM images of the microstructures correspond-

ing to cross sections perpendicular to the solidification direction are shown in Figure 1. In every case we observe continuous networks of single-crystal Al_2O_3 phase (dark contrast) and single-crystal based lanthanide and aluminium oxide compounds (Fig 1 a/ GAP = GdAlO_3 , b/ EAP = EuAlO_3 , c/ EAG = $\text{Er}_3\text{Al}_5\text{O}_{12}$, d/ YAG = $\text{Y}_3\text{Al}_5\text{O}_{12}$)

The two phases interpenetrate without grain boundaries, pores or colonies. These complex microstructures are consistent with other observations reported in literature [1,2]. The average phase domain size (length of the short axis of each domain) does not vary greatly for Al_2O_3 - Ln_2O_3 eutectics. But we can note that the Al_2O_3 -YAG composite exhibits a microstructure about five times larger. For all composites the microstructure size does not change on a large central part of rods when solidification rates are lower than 20 mm.h⁻¹. Above this value, colony microstructure begins to appear (Fig. 2). However we observed a decrease of this domain width towards the edge of the rod when specimen are prepared using the arc image furnace technique. This

Table 1

Al_2O_3	corundum struct. hexagonal symmetry, R-3c	$a=0.47591\text{nm}$	$c=1.29916\text{nm}$	
LnAlO_3	perovskite-type struct., orthorhombic symmetry, Pnma	a (nm)	b (nm)	c (nm)
$\text{Ln} = \text{Gd}$	GAP	0.53063	0.74452	0.52580
$\text{Ln} = \text{Eu}$	EAP	0.52877	0.74599	0.52775
$\text{Ln}_3\text{Al}_5\text{O}_{12}$	garnet-type struct. cubic symmetry, Ia3d	a (nm)		
$\text{Ln}=\text{Y}$	YAG	1.20065		
$\text{Ln}=\text{Er}$	EAG	1.19867		
$\text{Ln}=\text{Dy}$	DAG	1.20594		

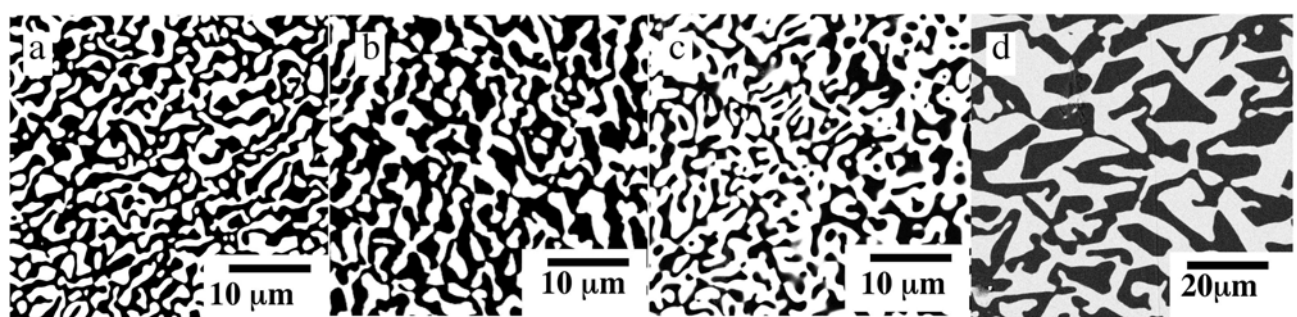


Fig. 1

decrease is directly related to the heating method which induces a radial temperature gradient higher than the Bridgman method.

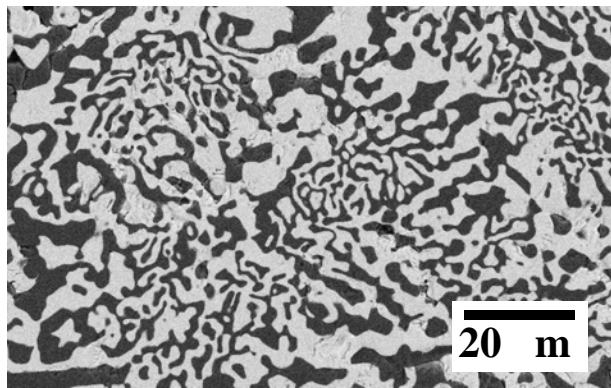


Fig. 2

SEM observations of sections parallel to the growth direction have a similar three-dimensional configuration of the microstructure.

Electron diffraction studies were performed on thin plates cut perpendicularly to the rod axes. They reveal that growth directions of these eutectics follow well-defined crystallographic axes. The orientations are usually unique. Two preferred orientations were determined for Al_2O_3 only depending on the used solidification process: $[10\bar{1}0]$ when specimen are grown by the floating zone method and $[11\bar{2}3]$ when the Bridgman method is employed. The

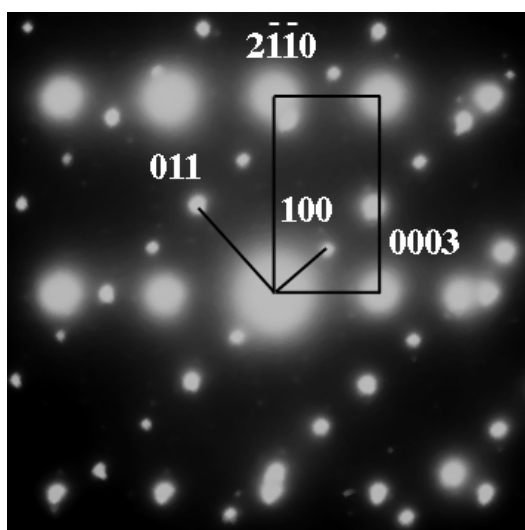


Fig. 3

electron diffraction pattern on figure 3 was performed on a platelet perpendicular to the $[10\bar{1}0]$ growth direction of a Al_2O_3 -GAP eutectic. The selected area is centred on the interface, and diffraction spots of both phases are superimposed on the same pattern. Crystallographic principal directions are strictly aligned according to the following epitaxial relations:

$$\begin{aligned}[10\bar{1}0] \text{Al}_2\text{O}_3 &\parallel [01\bar{1}] \text{Ln AlO}_3 \\ [2\bar{1}\bar{1}6] \text{Al}_2\text{O}_3 &\parallel [100] \text{Ln AlO}_3\end{aligned}$$

The growth directions and orientation relationships are summarized in Table 2 for the as-prepared eutectics.

Table 2

Eutectic phases	Al_2O_3 - LnAP	Al_2O_3 - LnAG
Growth directions	$[10\bar{1}0]\text{Al}_2\text{O}_3$ $\parallel [01\bar{1}]\text{LnAP}$	$[10\bar{1}0]\text{Al}_2\text{O}_3$ $\parallel [110]\text{LnAG}$
Orientation relationships	$(2\bar{1}\bar{1}0)\text{Al}_2\text{O}_3$ $\parallel (211)\text{LnAP}$	$(0001)\text{Al}_2\text{O}_3$ $\parallel (1\bar{1}2)\text{LnAG}$

These results were obtained from TEM patterns corresponding to local observations (some micrometers). In order to control the single-crystal homogeneity in large areas of the specimen, the EBSD technique has been used.

Figure 4, corresponding to the Al_2O_3 -YAG eutectic, shows orientation and Inverse

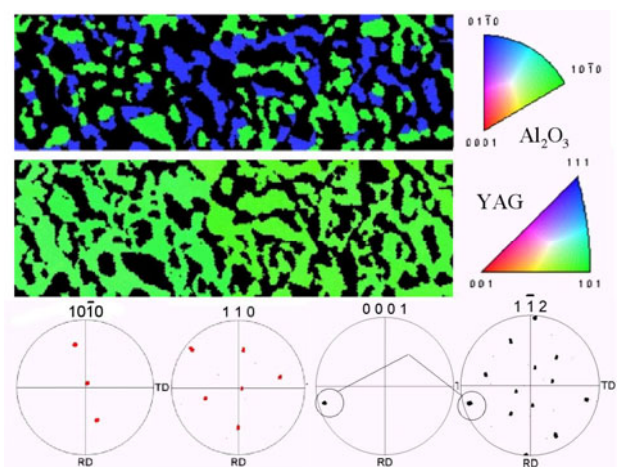


Fig 4

Pole Figures (IPF) maps in which the colors correspond to the crystal orientation as shown in the stereographic projection. For example, crystals with their 111 axis normal to the surface of the sample will be blue, and so on. The nearly alignment of $<10\bar{1}0>$ and $<110>$ crystallographic orientations with the N_d direction, normal to the observed surface (center of the stereo projection), is in good agreement with the growth directions reported in Table 2.

The orientation image maps ($150 \times 36 \mu\text{m}$) presented on figure 4 reveal the sample texture and the nearly single crystalline homogeneity of the sample. A unique colour corresponds to the YAG phase exhibiting one growth direction featuring and the absence of grain boundary. Two different colours are visible for alumina. They correspond to the same $\{10\bar{1}0\}$ orientation revealing two twin-related variants of Al_2O_3 . The non-centrosymmetry of the corundum structure gives rise to $[10\bar{1}0]$ and $[01\bar{1}0]$ crystallographic non-equivalent directions which cannot be distinguished by electron diffraction. Comparison of the Al_2O_3 and YAG pole figures leads to the same crystallographic relationships than those determined by TEM (Table 2).

3.2 Ternary systems

We showed in the previous section that the microstructure of the composite, in different oxide binary systems, could be controlled by unidirectional solidification. A high flexural strength, thermal stability and creep resistance of some of these binary eutectics have been reported in the literature. To increase the

fracture toughness of these materials we added a third phase (ZrO_2). For each system we prepared MGC at the eutectic composition in the $\text{Al}_2\text{O}_3/\text{ZrO}_2/\text{Ln}_2\text{O}_3$ ternary phase diagrams. After solidification, the phases identified by X-ray diffraction consist of an alumina phase, a perovskite (or garnet) phase and a Ln-containing fully-stabilized cubic ZrO_2 . The starting eutectic compositions, unit-cell parameters of constituent phases and the composition of zirconia phase are gathered in Table 3.

Table 3

65 Al_2O_3 - 19 ZrO_2 - 16 Y_2O_3 (mol%)		
Al_2O_3 $a=0.4758\text{nm}$ $c=1.2997\text{nm}$	YAG $a=1.2005\text{nm}$	ZrO_2 (15.5 mol% Y_2O_3) $a=0.5165\text{ nm}$
65.9 Al_2O_3 - 18.6 ZrO_2 - 15.5 Er_2O_3 (mol%)		
Al_2O_3 $a=0.4759\text{nm}$ $c=1.2999\text{nm}$	EAG $a=1.1983\text{nm}$	ZrO_2 (15.3 mol% Er_2O_3) $a=0.5159\text{ nm}$
58 Al_2O_3 - 23 ZrO_2 - 19 Gd_2O_3 (mol%)		
Al_2O_3 $a=0.4759\text{nm}$ $c=1.2993\text{nm}$	GAP $a=0.53022\text{nm}$ $b=0.74418\text{nm}$ $c=0.52541\text{nm}$	ZrO_2 (16 mol% Gd_2O_3) $a=0.5200\text{ nm}$

The amount of $\text{Ln}(\text{orY})_2\text{O}_3$ as solid solution in ZrO_2 was determined from X-Ray patterns using a Vegard's law [10]. Transverse sections of different ternary eutectics containing Y_2O_3 (a), Er_2O_3 (b) and Gd_2O_3 (c) are shown in Figure 5. Firstly, we can note, that morphology of the garnet-type phase is modified depending on the oxide added to alumina

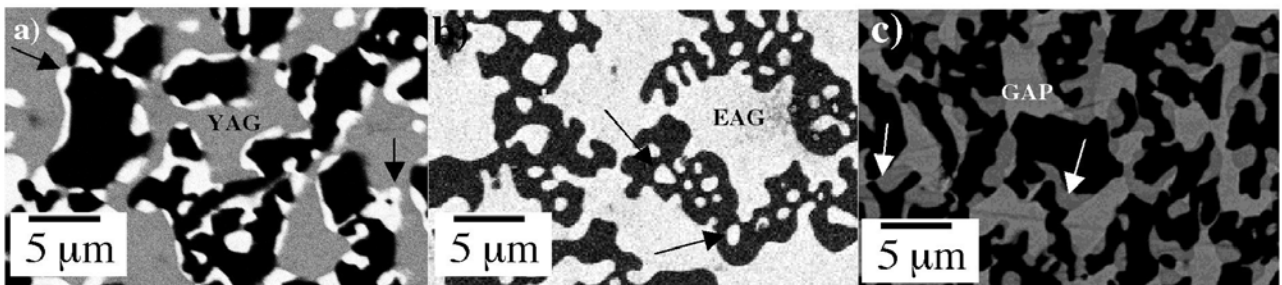


Fig. 5

and zirconia (indicated by arrows). At the same solidification rate, large facets are developed for the ternary eutectic with Ln=Er at the contrary of composites containing Y. Secondly, in the case of based-yttrium eutectic, zirconia phase is always grown at the interface between Al_2O_3 and YAG. When Ln=Er, cubic zirconia dispersoids are observed not only at the interfaces but also in the alumina phase. A similar microstructure was observed for yttrium based eutectics prepared by the Bridgman technique at higher solidification rates. Electron diffraction patterns (Fig. 6) performed on the interfaces of the eutectic phases reveal the epitaxial relationships on the one hand between Al_2O_3 and ZrO_2 (left image) and on the other between Al_2O_3 and $\text{Y}_3\text{Al}_5\text{O}_{12}$ (right image).

We determined the following relationships:

$$[10\bar{1}0]\text{Al}_2\text{O}_3//[001]\text{YAG}//[001]\text{ZrO}_2$$

corresponding to growth directions of each phase coupled with relative orientations :

$$(0001)\text{Al}_2\text{O}_3//(100)\text{ZrO}_2$$

and

$$(0001)\text{Al}_2\text{O}_3//(100)\text{YAG}$$

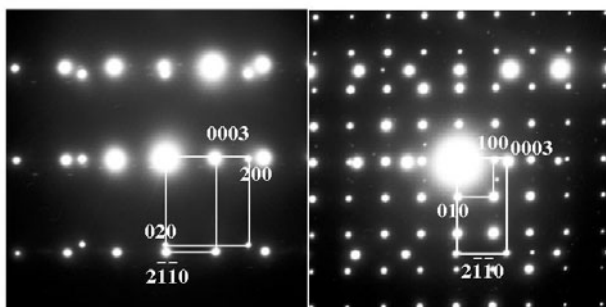


Fig. 6

The orientation relationships between alumina and cubic zirconia are strictly similar to those determined in previous papers for the $\text{Al}_2\text{O}_3\text{-ZrO}_2$ binary eutectic [11]. Crystallographic orientations of three phases are verified for large areas of the specimen as shown on IPF images which reveal unique growth directions on $2 \times 2 \text{mm}^2$ zones and relative orientations in good agreement with electron diffraction studies (Fig. 7)

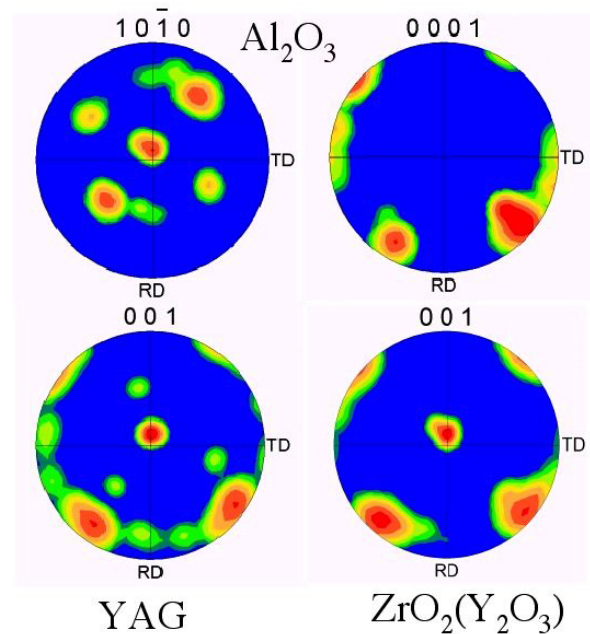


Fig. 7

3.3 Mechanical properties

As reported in the paragraph before, addition of zirconia to binary eutectics modifies solidification conditions and consequently the microstructure of the final composite. However the single-crystal homogeneity of the material is not changed. Orientation relationships between zirconia and the two others eutectic phases which were revealed involves low-energy interfaces.

We investigated the influence of that addition on hardness and fracture toughness of these materials at room temperature. Hardness values measured with a Vickers indent are reported in Table 4. \perp and $//$ symbols indicate that measurements were carried out on sections perpendicular and parallel to the growth direction.

The mean value of hardness varies very little whatever the considered oxides system. Fracture toughness values calculated from the length of cracks reveals following features :

- binary eutectics have a fracture toughness higher than Al_2O_3 and close to known values for $\text{Al}_2\text{O}_3\text{-ZrO}_2$ composites [12].
- lower is the mean size of the microstructure higher is the K_{IC} value ($\text{Al}_2\text{O}_3\text{-YAG} < \text{Al}_2\text{O}_3\text{-EAG} < \text{Al}_2\text{O}_3\text{-GAP}$).

- addition of zirconia induces a noticeable toughening effect. This effect is more important for the systems associating alumina and garnet type structure. The estimated value of K_{IC} increases from 6 to 10 MPa.m^{1/2}.
- K_{IC} values perpendicular or parallel to growth directions are very similar in good agreement with the isotropy of the microstructure and do not seem dependent of crystallographic orientation.

Table 4

System	Hv (GPa)	K_{IC} (MPa.m ^{1/2})
Al ₂ O ₃ -YAG (⊥)	21.8	5.2
Al ₂ O ₃ -EAG (⊥)	16.9	6.2
Al ₂ O ₃ -ZrO ₂ -YAG (⊥)	18.4	9.8
Al ₂ O ₃ -ZrO ₂ -YAG (//)	19.8	8.9
Al ₂ O ₃ -ZrO ₂ -EAG (⊥)	18	10
Al ₂ O ₃ -GAP (⊥)	15.9	7.5
Al ₂ O ₃ -ZrO ₂ -GAP (⊥)	17.9	8.5

4. Conclusion

Interconnected microstructures were obtained from based-oxide binary and ternary systems using two different growth methods. Whatever the used method, morphology of microstructures does not change. The floating zone method allows to grow composites at solidification rates higher than the Bridgman method due to a higher thermal gradient but the microstructure displays a lower homogeneity on the external zones of the as-prepared rods. Preferred growth directions and crystallographic orientation relationships between constituents phases were revealed for all the investigated eutectics. The EBSD technique allowed to show the single-crystal feature of

grown composites. The addition of zirconia corresponding to ternary eutectic compositions led to an increase of fracture toughness.

References

- [1] Waku Y, Nakagawa N, Wakamoto T, Ohtsubo H., Shimizu K & Kohtoku Y. A ductile ceramic eutectic composite with high strength at 1873K, *Nature*, 389, pp 49-52, 1997
- [2] Waku Y, Nakagawa N, Wakamoto T, Ohtsubo H., Shimizu K & Kohtoku, High temperature strength and stability of unidirectionally solidified Al₂O₃/YAG eutectic composite, *J. Mater. Sci.* 33, pp1217-1225, 1998
- [3] Revcolevschi A., Dalhenne G. and Michel D. Interfaces in directionally solidified oxide-oxide eutectics, *External and internal interfaces of metal oxides*, Materials Science Forum, Trans. Tech. Publications, pp 173-197, 1988
- [4] Cooksay D.J.S., Munson D., Wilkinson M.P., Hellawell A.H., Freezing of some continuous binary eutectic mixtures, *Phil. Mag.*, 10, pp 745-769, 1964.
- [5] Hunt J.D and Jackson, K.A. Binary eutectic solidification, *Trans AIME*, 236, pp 843-852, 1966
- [6] Mollard F.R. and Flemings M.C., Growth of composites from the melt, *Trans AIME*, 239, pp 1526-1546, 1967.
- [7] Frazer C.S., Dickey Ec., Sayir, A., Crystallographic texture and orientation variants in Al₂O₃-Y₃Al₅O₁₂ directionally solidified eutectic crystals, *Journal of crystal growth*, 233, pp 187-195, 2001
- [8] Revcolevschi A., Arc image furnace for X-Ray diffraction studies to 3000°C and high temperature crystal growth, *Rev. Int. Hautes Temp. Refract.*, 7, pp 73-90, 1970.
- [9] Evans A.G., Charles E.A. Fracture Toughness Determination by Indentation *J. Am. Ceram. Soc.* 59, pp 371-372, 1976.
- [10] Yashima M., Ishisawa N., Yoshimura M. Application of an Ion-Packing on Defects Clusters to Zirconia Solid Solutions : II, Applicability of Vegard's law *J. Am. Ceram. Soc*, 75, pp 1550-1557, 1992
- [11] Mazerolles, L., Michel D. and Portier, R., Interfaces in oriented Al₂O₃-ZrO₂ (Y₂O₃) eutectics, *J. Am. Ceram. Soc*, 69, pp 252-255, 1986
- [12] Lange F.F. Transformation Toughening, Part 4, *J. Mat. Sci.* 17 pp 247-254, 1982